Third International Conference on CFD in the Minerals and Process Industries
CSIRO, Melbourne, Australia
10-12 December 2003

COMPUTATIONAL FLUID DYNAMIC SIMULATIONS OF CHEMICALLY REACTIVE FLUIDIZED BED PROCESSES

Thomas J. O'BRIEN[1], Madhava SYAMLAL[2], and Chris GUENTHER[2]

[1]National Energy Technology Laboratory, 3610 Collins Ferry Road,
Morgantown, WV, 26507-0880, USA
[2]Fluent, Inc., 3647 Collins Ferry Road,
Morgantown, WV 26507, USA

ABSTRACT

There has been extensive progress in the use of multiphase computational fluid dynamics (CFD) for the simulation of reactive fluidized beds. Several case studies (ozone decomposition, silane/tetrachlorosilane pyrolysis, methane combustion, and coal gasification) are presented which demonstrate the current capabilities, using the NETL developed code MFIX. For the ozone studies, thermal effects are unimportant; the ozone is only present in small amounts. Also, mixing effects are not addressed since the ozone was premixed with the fluidization air. For methane combustion, the chemical reactions are all in the gas phase although heat transfer to the granular phase is important; again the reactants are premixed in the plenum. For coal gasification, the solids must be mixed with the fluidizing air; many heterogeneous reactions are also included. Complicated chemical schemes are required to describe these processes; the heat release is accounted for, as is the effect on fluidization of gas released by the chemical conversion.

NOMENCLATURE

F_{gm} drag coefficient between gas and phase m ≥ 1

H_{gm} heat transfered between gas and phase m ≥ 1

H_{wall} heat transfered between gas and the wall

ΔH_{rm} heat of reactions in phase m

$\vec{I}_{gm}$ momentum exchange between gas and phase m ≥ 1

$\vec{I}_{ml}$ momentum exchange between granular phases m,l ≥ 1

$\vec{q}_m$ conductive heat flux in phase m

R_{mn} reaction rate of species n in phase m

R_{gm} total reaction rate between phase m and gas phase

$\overline{\overline{S}}_m$ stress in phase m: gas (m = 0) or granular (m ≥ 1)

T_m temperature of phase m

T_{wall} temperature of vessel wall

$\vec{v}_m$ local instantaneous velocity of phase m

X_{mn} mass fraction of species n in phase m

ε_m volume fraction of phase m

ρ_m density of phase m

INTRODUCTION

There has been extensive progress in the use of multiphase computational fluid dynamics (CFD) for the simulation of isothermal, nonreactive fluidized beds (Snider, O'Rourke, and Andrews, 1998, Guenther and Syamlal, 2000; McKeen and Pugsley, 2003). The utility of this computation approach is here demonstrated for chemically reactive flows with heat transfer, using the NETL developed code MFIX. Several case studies (ozone decomposition, silane/tetrachlorosilane pyrolysis, methane combustion, and coal gasification) are presented which demonstrate the current capabilities. Previous calculations accurately simulated experimental results for ozone decomposition in a bubbling fluidized bed. However, thermal effects were not important, since the ozone was only present in small amounts; also, mixing effects were not addressed since the ozone was premixed with the fluidization air in the plenum The additional calculations reported in this paper are for processes that are very exothermic. For methane combustion, the chemical reactions are all in the gas phase; for coal gasification and the Si processes, there are also many heterogeneous reactions. In addition to the complicated chemical schemes required to describe these processes, the heat release is accounted for, as is the effect on fluidization of gas released by the chemical conversion. In order to allow this coupled calculation, advanced computational methods, which were developed for single phase CFD, have been utilized. These calculations resolve many interesting features of the processes, such as regions of preferred bubble transit, which allow gas by-passing, and chemically reactive zones near the distributor.

MODEL DESCRIPTION

MFIX Equation Set

The multifluid model using in these simulations describes the carrier fluid and each granular type as an interpenetrating fluid. (Anderson and Jackson, 1967; Syamlal, Rogers and O'Brien, 1993). The code MFIX

(www.mfix.org) solves the following set of partial differential equations in a sequential fashion.

Gas (m = 0) or Granular Phase (m ≥ 1) Continuity Eq.:

$$\frac{\partial}{\partial t}(\varepsilon_m \rho_m) + \nabla \cdot (\varepsilon_m \rho_m \vec{v}_m) = \sum_{n=1}^{N_g} R_{mn}$$

Species Mass Balance:

$$\frac{\partial}{\partial t}(\varepsilon_m \rho_m X_{mn}) + \nabla \cdot (\varepsilon_m \rho_m X_{mn} \vec{v}_m) = R_{mn}$$

Gas Phase (m = 0) Momentum Eq:

$$\frac{\partial}{\partial t}(\varepsilon_g \rho_g \vec{v}_g) + \nabla \cdot (\varepsilon_g \rho_g \vec{v}_g \vec{v}_g) = \nabla \cdot \bar{\bar{S}}_g + \varepsilon_g \rho_g \vec{g} - \sum_{l=1}^{M} \vec{I}_{gm}$$

Granular Phase (m ≥ 1) Momentum Eq:

$$\frac{\partial}{\partial t}(\varepsilon_m \rho_m \vec{v}_m) + \nabla \cdot (\varepsilon_m \rho_m \vec{v}_m \vec{v}_m) = \nabla \cdot \bar{\bar{S}}_m + \varepsilon_m \rho_m \vec{g} + \vec{I}_{gm} - \sum_{l=1, l\neq m}^{M} \vec{I}_{ml}$$

Gas Phase Temperature Eq:

$$\varepsilon_g \rho_g C_{pg} \left(\frac{\partial T_g}{\partial t} + \vec{v}_g \cdot \nabla T_g \right) = -\nabla \cdot \vec{q}_g - H_{g1} - H_{g2} - \Delta H_{rg} + H_{wall}(T_{wall} - T_g)$$

Granular Phase (m ≥ 1) Temperature Eq:

$$\varepsilon_m \rho_m C_{pm} \left(\frac{\partial T_m}{\partial t} + \vec{v}_m \cdot \nabla T_m \right) = -\nabla \cdot \vec{q}_m + H_{gm} - \Delta H_{rm}$$

These equations are supplemented by a host of constitutive relations which are required for closure, some of which are listed below, roughly in order of their significance.

Momentum Exchange:

$$\vec{I}_{gm} = -\varepsilon_m \nabla P_g - F_{gm}(\vec{v}_m - \vec{v}_g) + R_{gm}\left[\xi_{gm} \vec{v}_m + \bar{\xi}_{gm} \vec{v}_g\right]$$

The contributions to this term are the buoyancy effect of the fluidizing gas, the gas-granular drag law and the momentum exchange associated with mass transfer between the phases.

Gas-Particle Drag:

$$F_{gm} = \frac{3}{4} \frac{\varepsilon_m \varepsilon_g \rho_g}{V_{rm}^2 d_{pm}} C_{Dm}\left(\frac{Re_m}{V_{rm}}\right)\left|\vec{v}_m - \vec{v}_g\right|$$

$$V_{rs} = 0.5\left(A - 0.06 Re_s + \sqrt{(0.06 Re_s)^2 + 0.12 Re_s (2B - A) + A^2}\right)$$

$$A = \varepsilon_g^{4.14}, \qquad B = \begin{cases} c\,\varepsilon_g^{1.28} & \text{if } \varepsilon_g \le 0.85 \\ \varepsilon_g^{d} & \text{if } \varepsilon_g > 0.85 \end{cases}$$

Gas-Phase Stress:

$$\bar{\bar{S}}_g = -P_g \bar{\bar{I}} + 2\varepsilon_g \mu_g \bar{\bar{D}}_g + \varepsilon_g \lambda_g \mathrm{tr}(\bar{\bar{D}}_g)\bar{\bar{I}}$$

Granular Phase Stress:

$$\bar{\bar{S}}_s = \begin{cases} -P_s^p \bar{\bar{I}} + \bar{\bar{\tau}}_s^p & \text{if } \varepsilon_g \le \varepsilon_g^* \\ -P_s^v \bar{\bar{I}} + \bar{\bar{\tau}}_s^v & \text{if } \varepsilon_g > \varepsilon_g^* \end{cases}$$

For values of $\varepsilon_g > \varepsilon_g^*$, the "viscous" stress is represented by the kinetic theory of granular material

$$P_s^v = K_1 \varepsilon_s^2 \Theta_s$$

$$K_1 = 2(1+e)\rho_s g_0$$

$$\bar{\bar{\tau}}_s^v = 2\mu_s^v \bar{\bar{D}}_s + \lambda_s^v \mathrm{tr}(\bar{\bar{D}}_s)\bar{\bar{I}}$$

$$\mu_s^v = K_3 \varepsilon_s \sqrt{\Theta_s}$$

$$\lambda_s^v = K_2 \varepsilon_s \sqrt{\Theta_s}$$

$$K_3 = \frac{d_p \rho_s}{2}\left\{\frac{\sqrt{\pi}}{3(3-e)}\left[1 + 0.4(1+e)(3e-1)\varepsilon_s g_0\right] + 8\varepsilon_s g_0 (1+e)/5\sqrt{\pi}\right\}$$

Granular Psuedo-Temperature:

$$2K_4 \varepsilon_s \Theta^{1/2} = -K_1 \varepsilon_s tr(\bar{\bar{D}}_s) + \sqrt{K_1^2 \varepsilon_s^2 tr^2(\bar{\bar{D}}_s) + 4K_4 \varepsilon_s \left[K_2 tr^2(\bar{\bar{D}}_s) + 2K_3 tr(\bar{\bar{D}}_s^2)\right]}$$

For more compacted conditions, $\varepsilon_g \le \varepsilon_g^*$, a "plastic" stress representation is used.

$$P_s^p = 10^{25}(\varepsilon_s - \varepsilon_s^{cp})^{10},$$

$$\bar{\bar{\tau}}_s^p = 2\mu_s^p \bar{\bar{D}}_s$$

$$\mu_s^p = P_s^p \sin\phi / 2\sqrt{I_{2D}}.$$

$$I_{2D} = D_{s12}^2 + D_{s23}^2 + D_{s31}^2 + \frac{1}{6}\left((D_{s11} - D_{s22})^2 + (D_{s22} - D_{s33})^2 + (D_{s33} - D_{s11})^2\right)$$

Gas Phase Convective Heat Flux:

$$\vec{q}_g = -\varepsilon_g k_g \nabla T_g$$

A Fickian approximation is used.

Gas-Granular Heat Transfer Coefficient:

$$H_{gm} = -\gamma_{gm}\left(T_m - T_g\right)$$

CHEMICALLY REACTIVE SYSTEMS

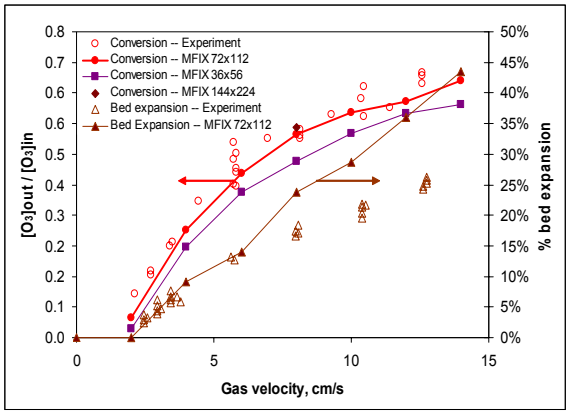

Figure 1: Ozone decomposition, $[O_3]_{out}/[O_3]_{in}$, (left scale; circles) and fractional bed expansion (right scale; triangles) as a function of fluidization velocity. Open symbols are simulations at different mesh resolutions (connected by solid lines); data are solid symbols, reported by Fryer and Potter (1976).

Ozone Decomposition has been used extensively to characterize the contacting in fluidized beds. An extensive study (Syamlal and O'Brien, 2003) was based on the experiments conducted by Fryer and Potter (1976) in a 22.9 cm diameter cylinder, 200 cm tall. The first order global kinetics for the heterogeneous decomposition reaction $O_3 \rightarrow 2/3\ O_2$ was represented as $R_{O_3} = -3R_{O_2}/2 = -k\,\varepsilon_s \rho_g X_{O_3}/MW_{O_3}$. The catalytic rate constant k was determined by experimental measurements in a fixed bed (Fryer and Potter, 1976). These simulations very accurately reproduced the over-all decomposition of ozone over a range of fluidization velocities, provided the numerical resolution was sufficient to capture bubble formation accurately. At low resolution (shown as MFIX 36x56, in Figure 1), the calculated bubbles still contained considerable amounts of the granular phase so that contacting occurred even in these regions. Hence, the decomposition was over-estimated. However, with increased numerical resolution, the conversion was predicted quite accurately over a broad range of fluidization velocities (Figure 1., MFIX 72x112). One condition was calculated at even higher resolution to confirm that the conversion results were converged (Figure 1., MFIX 144x224). As the fluidization velocity was increased, bubble formation increased; this resulted in decreased decomposition since more of the ozone by-passed the bed. With adequate numerical resolution, these simulations show that this global feature can be captured quantitatively. At the higher velocities, the agreement with the reported bed expansion began to deteriorate. It is not know whether this was due to increased experimental uncertainty, as noted (Fryer and Potter, 1976), or because even higher numerical resolution is required to resolve the surface of a vigorously bubbling bed. In this study, since the ozone was only present in trace amounts, there were no thermal effects and no effect of the chemical reactions on the bed dynamics.

Silicon Chlorination is required to form trichlorosilane, the most common precursor for the commercial converstion of metallurgical grade Si to high purity, polycrystalline metallic silicon for the electronics industry (JPL, 1979). Experimental rate information was analyzed in terms of a two step global reaction scheme which was used in the simulation. The initial step is a slow homogeneous gas-phase reaction, $SiCl_4 + H_2 \leftrightarrow SiHCl_3 + HCl$, represented as

$$R_{\mathrm{TCS-homo}} = 0.267/T_g^{1/2}\ e^{-27{,}680/T_g} \times \left[P_{STC}\,P_{H_2}^{1/2} - P_{TCS}\,P_{HCl}/\left(K_{EQ}\,P_{H_2}^{1/2}\right)\right]$$

(In this expression, the partial pressures are expressed in g/(cm·s^2) and the temperature is in Kelvin.) The dimensionless thermodynamic equilibrium constant is written as $K_{EQ} = \exp\left(4.2873 - 8790.7/T_g\right)$. This reaction is complemented by a fast heterogeneous reaction, $Si(s) + 3\ HCl \rightarrow SiHCl_3 + H_2$, represented by

$$R_{\mathrm{TCS-hetero}} = 1.698\times10^{-3}\left(6\left(1-\varepsilon_g\right)/d_p\right) \times e^{-11{,}575/T_g}\left[P_{HCl}\right]^{1/2}$$

Silane Pyrolysis in a fluidized bed is the final step in a proposed process for the formation of ultrapure silicon from metallurgical grade (m.g.) silicon. (JPL, 1979; Caussat, Hémati, and Couderc, 1995-I). In simulating this process, the heterogeneous decomposition, $SiH_4(g) \rightarrow Si(s) + 2H_2(g)$ was represented by a global reaction (Furusawa, Kojima, and Hiroha, 1988)

$$R_{SiH_4} = \frac{6(1-\varepsilon_g)2.1510^{10}e^{-23016/T}[SiH_4]}{d_p\left(1+0.034P_{H2}+0.0076e^{(3954/T)}P_{SiH4}\right)}$$

Using a more complicated mechanism (Caussat, Hémati, and Couderc, 1995-II) produced similar results. These simulations of the 63 x 5.3 cm (ID) reactor reproduced the reported production of H_2 in the exit stream (Caussat, Hémati, and Couderc, 1995-I), but this was not a very sensitive test of the accuracy of the simulations. The reaction was essentially completed in a 5 cm region above the distributor. It was significant that the results for 2-D (cylindrically symmetric) and 3-D simulations showed significantly different behaviour for this narrow geometry. The 2-D simulation restricted the motion of bubbles to the centreline so that there was a strong radial variation in the time-averaged voidage. In the 3-D simulations, the bubbles migrated to the centreline, resulting in a much more uniform voidage distribution. This had a significant effect on the detailed chemical profiles within the bed (but not the overall conversion), since the decomposition rate depends on the local particle loading.

Methane Combustion in fluidized beds has been experimentally studied by many groups (*e.g.*, Hesketh and Davidson, 1991; van der Vaart, 1992; Pre, Hemati, and Marchand, 1998). It was decided to simulate the experiments of (van der Vaart, 1992) since information on both the hydrodynamic behaviour of the bed and the combustion were reported. In an initial calculation, the chemical species transport equations and the energy

equation where deactivated to examine only the hydrodynamic behaviour of a nonreactive bed. In this simulation, after an initial transient, flat void regions formed very close to the distributor and then rolled up into the characteristic shape of "bubbles," mainly near the outside, bottom corner of the vessel. Once formed, these bubbles rose and migrated toward the centreline of the bed. On average, this generated a sloping band of reduced void fraction from the lower outside region of the vessel toward the centreline, producing a region of high gas flow, related to gas by-passing the bed in the "bubble phase." The bubble-induced time-averaged solids motion showed a downward circulation pattern near the centreline; near the top of the bed, there was also downward flow of solids near the outside wall. The bed was not deep enough to establish an upwards solids circulation pattern near the centerline; bubbles did not have enough time to migrate completely to the center of the bed before bursting at the surface. This type of pattern is typical of shallow bubbling beds (Kunii and Levenspiel, 1991).

The conditions of the van der Vaart experiments correspond to the "fast" bubble regime; the voidages rise through the bed faster than the interstitial fluid flow. Thus, the by-passing gas makes contact with emulsion phase only in the "cloud" region surrounding the bubble. This may delay the heating of the inlet gas by the bed material. As the superficial velocity increases, so does the bubble size, which implies their rise velocity increases so that the cloud is further reduced. This further delays the gas heat-up.

This process of combustion involves chemical reactions, which are all in the gas phase. However, the granular phase exerts a significant influence by quenching the free radicals and moderating temperature changes. It is difficult to quantify the extent of these effects. A global kinetics scheme was used in the simulation, based on a simple two step combustion scheme:
1) $CH_4 + 3/2\ O_2 \rightarrow CO + 2\ H_2O$
2) $CO + ½O_2 \rightarrow CO_2$.
This includes six gas phase species: CH_4, CO_2, CO, H_2O, O_2, and N_2. The homogeneous reaction rates used were those of Dryer and Glassman (1973)

$$R_{CH_4} = -\varepsilon_g 10^{13.2}\, e^{-48{,}400/RT} \left[CH_4\right]^{0.7} \left[O_2\right]^{0.8}$$

$$R_{CO_2} = \varepsilon_g 10^{14.75}\, e^{-43{,}000/RT} \left[CO\right]^{1.0} \left[H_2O\right]^{0.5} \left[O_2\right]^{0.25}$$

A factor of ε_g has been included in these expressions to convert the reported rate expressions from gas-volume to reactor-volume basis. These rate expression had to be changed in another significant manner, however, to account for quenching of free radicals by the granular phase, as discussed below.

The experimental data (van der Vaart, 1992) shows that methane is consumed rather gradually over a height of about 13 cm above the distributor. In stark contrast the simulations showed that methane was consumed almost immediately (in less than 1 cm) above the distributor. This is thought to be because the above rate expressions, developed for gas-phase combustion, do not account for combustion inhibition (caused by free-radical quenching on particle surfaces) observed in packed beds (Hayhurst and Tucker, 1990; Srinivasan *et al.*, 1998). Since we are not aware of any global rate expression that accounts for this effect we chose the *ad hoc* solution of "turning off" the reactions in regions where the solids volume fraction exceeded 0.1. With this modification, the predicted methane profile was in better agreement with experiment. Although these calculations demonstrated that such a simulation is feasible, the agreement with the experimental results is incomplete since there is such great uncertainty in the reaction rates.

Coal Gasification: For coal gasification, in addition to the effect of heat release, there are also many heterogeneous reactions which require accounting for the effect on fluidization of the gas released by the chemical conversion. The chemical kinetics scheme used to describe coal gasification, although global, is still quite complicated, tracking 8 gas phase species and 4 solid phase species (Syamlal and Bisset, 1992):

Drying: Moisture (coal) → H_2O(g)

$$R_{Drying} = 1.1\times10^5\, e^{-21200/RT_s}\ \varepsilon_s\, \rho_s\, X_{sH20}$$

Devolatilization:

Volatile Matter → β_d^{Tar} Tar + β_d^{CO} CO + β_d^{CO2} CO_2 + β_d^{CH4} CH_4 + β_d^{H2} H_2 + β_d^{H2O} H_2O

For $X_{sVM} \geq X^*$,

$$R_{Devol} = 1.1\times10^5\, e^{-21200/RT_s}\ \varepsilon_s\ \rho_s (X_{sVM} - X^*)$$

Otherwise, $R_{Devol} = 0$. Here

$$X^* = (X^0_{sVM}/100)\left(867.2/(T_s - 273)\right)^{3.914}$$

for $T_s < 1223$; otherwise, $X^* = 0$.

Tar-cracking:

Tar → α_c Fixed Carbon + β_c^{CO} CO + β_c^{CO2} CO_2 + β_c^{CH4} CH_4 + β_c^{H2} H_2 + β_c^{H2O} H_2O

$$R_{crack} = 2.5\times10^7\, e^{29000/RT_g}\ \varepsilon_g\, \rho_g\, X_{gTar}$$

Steam gasification: $C + H_2O \rightarrow CO + H_2$

$$R_{steam} = 77.5\times e^{45000/RT_g}\ \varepsilon_s \rho_s X_{sC} (p_{H_2O} - p^*_{H_2O})$$

where

$$p^*_{H_2O} = \left(p_{H_2}\, p_{CO}\right) e^{(-17.29+16326/T_g)}$$

CO_2 gasification: $C + CO_2 : 2CO$

$$R_{CO_2\ gas} = 77.5 e^{-45000/RT_g}\ \varepsilon_s \rho_s X_{sC} (p_{CO_2} - p^*_{CO_2})$$

Methanation: $C + 2H_2 :\ CH_4$

$$R_{meth} = e^{-7.087-8078/T_g}\left(\varepsilon_s \rho_s X_{sC}/12\right)\left(p_{H_2} - p^*_{H_2}\right)$$

$$p^*_{H_2} = \sqrt{p_{CH_4} e^{(13.43-10999/T_g)}}$$

Carbon combustion: $2C + O_2 \rightarrow 2CO$

$$R_{C\,comb} = -6\,\varepsilon_s p_{O_2} \Big/ \left[d_p\left(k_f^{-1} + k_a^{-1} + k_r^{-1}\right)\right]$$

CO combustion: $CO + \frac{1}{2}O_2 \rightarrow CO_2$

$$R_{CO\,comb} = 3.98\times 10^{14} e^{-40000/RT_g} \times \varepsilon_g\left(\rho_g X_{gO_2}/32\right)^{0.25}\left(\rho_g X_{gCO}/28\right) \times\left(\rho_g X_{gH_2O}/18\right)^{0.5}$$

CH_4 combustion: $CH_4 + 2O_2 \rightarrow CO_2 + 2H_2O$

$$R_{CH_4\,comb} = 6.7\times 10^{12} e^{-48400/RT_g}\,\varepsilon_g \times\left(\rho_g X_{gO_2}/32\right)^{1.3}\left(\rho_g X_{gCH_4}/16\right)^{0.2}$$

H_2 combustion: $H_2 + \frac{1}{2}O_2 \rightarrow H_2O$

$$R_{H_2\,comb} = 1.08\times 10^{6} e^{-30000/RT_g} \times \varepsilon_g\left(\rho_g X_{gO2}/32\right)\left(\rho_g X_{gH2}/2\right)$$

Tar combustion: $Tar + f_{O2}\,O_2 \rightarrow f_{CO2}\,CO_2 + f_{H2O}\,H_2O$

$$R_{Tar\,comb} = 3.8\times 10^{11} e^{-30000/RT_g} \times \varepsilon_g\left(\rho_g X_{gO_2}/32\right)^{1.5}\left(\rho_g X_{gTar}/MW_{Tar}\right)^{0.25}$$

Water gas - shift reaction: $CO + H_2O : CO_2 + H_2$

$$R_{shift} = 2.877\times 10^{5}\, w_{g3} f_3 P^{(0.5-P/250)} e^{-27760/RT_g} \times\left(X_{gCO} X_{gH_2O} - X_{gCO_2} X_{gH_2}/K_3\right)$$

$$f_3 = \varepsilon_g(1-\varepsilon_g) X^0_{Ash}\ \rho_s e^{-8.91+5553/T_g}$$

$$K_3 = e^{-3.63061+3.95571/T_g}$$

Species	Simulation	Experimental
CO	13.0	11.9
CO_2	8.0	7.4
CO_2/ CO ratio	1.6	1.6
CH_4	1.9	1.1
H_2	7.0	6.5
H_2O	4.1	6.1
Carbon conv.	87%	95%
Exit T_g (K)	1707°F (1204 K)	1725°F (1214 K)

Table 1: Comparison between simulation results and experiments of the mole percent of the major species (CO, CO_2, CH_4, H_2, and H_2O), total carbon conversion and gas temperature in the exit product gas of a representative run of the Power System Development Facility transport reactor (Leonard, *et al.*, 2002).

Using this kinetic scheme, simulations have been performed of the large transport gasifier at Power System Development Facility, operated by Southern Company in Wilsonville, Alabama, USA (Leonard, *et al.*, 2002). Since this is an industrial scale facility, only limited detailed data is available for validation. Table 1 shows good agreement between the simulations (Guenther, *et al.*, 2002) and the experiments for the distribution of the major species in the product gas.

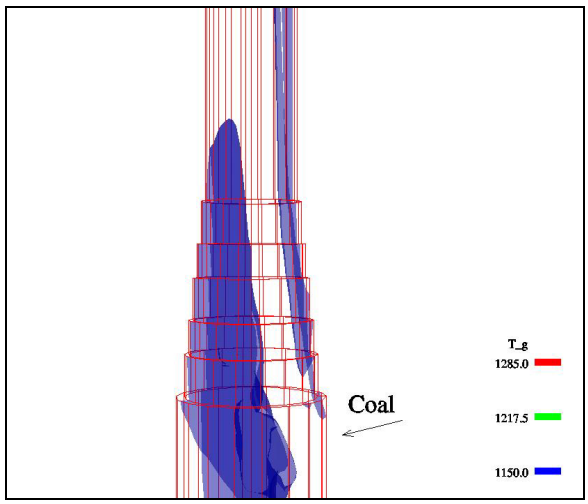

Figure 2: A view of the transition section of the Power System Development Facility transport reactor (Leonard, *et al.*, 2002), showing time-averaged isosurfaces of the mass fractions of oxygen (lower region; $X_{O2} = 0.1$) and hydrogen (upper region; $X_{H2} = 0.1$) generated at the coal inlet. The isosurfaces are colour coded according to the gas phase temperature.

Figure 2 shows a seven-foot view of the transition region in the gasifier, between the mixer section and the riser. Fresh coal is injected near the top of the mixer section. Isosurfaces are shown of the time-averaged mass fraction of O_2 (lower left region; $X_{O2} = 0.1$) and H_2 (narrow upper right region; $X_{H2} = 0.1$). The surfaces themselves are coloured corresponding to the local gas temperature, which is almost the same as the granular phase temperature except close to the coal inlet.

There are many uncertainties in these simulations. It is unknown if the mesh resolution accurately captures the multiphase hydrodynamics; mesh independent was not demonstrated. There is great uncertainty in the carbon content of the recycle solid stream in this facility, and the simulations are quite sensitive to this number. Also, the coal chemistry scheme contains many uncertain parameters. However, such a calculation demonstrates that it is possible to provide detailed information about the flow and chemical processes within a large industrial unit.

CONCLUSION

These examples of the simulation of chemically reactive fluidized bed processes demonstrate that it is feasible to calculate the coupled effects of heavily-loaded, gas-particle hydrodynamics, heat transfer and complicated chemical reactions. However, transient calculations are required to capture the inherent fluctuations in these flows. (Turbulence theories used in single phase flow have not been extended to describe these types of flows.) Thus,

these calculations are computationally very intensive, requiring days of CPU time on parallel clusters. Also, quite high numerical resolution is required to resolve the behaviour of the multiphase flow adequately so that the chemistry is represented accurately. This problem is, of course, compounded for large scale processes.

ACKNOWLEDGMENTS

This work was supported by the U.S. Dept. of Energy – Fossil Energy, National Energy Technology Center, and by U.S. Dept. of Energy – Energy Efficiency and Renewable Energy, Office of Industrial Technologies. The authors would like to thank the FE product manager Dr. Robert Romanosky and the EERE-OIT program manager Dr. Brian Valentine for their support.

REFERENCES

ANDERSON, T.B. and JACKSON, R., (1967), "A fluid mechanical description of fluidized beds," *Ind. & Eng. Chem. Fund.,* **6**, 527-539.

CAUSSAT, B., HÉMATI, M., and COUDERC, J.P., (1995), "Silicon deposition from silane or disilane in a fluidized bed – Part I: experimental study," *Chem. Eng. Science*, **50**, 3615-24.

CAUSSAT, B., HÉMATI, M., and COUDERC, J.P., (1995), "Silicon deposition from silane or disilane in a fluidized bed – Part II: theoretical analysis and modeling," *Chem. Eng. Science*, **50**, 3625-2435.

DRYER, F.L., and GLASSMAN, I., (1973), "High temperature oxidation of CO and CH_4," *14th Symposium (International) on Combustion*, The Combustion Institute, Pittsburgh, 987-1003.

FRYER, C., and POTTER, O.E., (1976), "Experimental investigation of models for fluidized bed catalytic reactors," *AIChE J.*, **22**, 38-47.

FURUSAWA, T., KOJIMA, T., and HIROHA, H., (1988), "Chemical vapor deposition and homogeneous nucleation in monosilane pyrolysis within interparticle spaces, application of fines formation analysis to fluidized bed CVD," *Chem. Eng. Science*, **43**, 2037-2042.

GUENTHER, C., and SYAMLAL, M., (2001), "The Effect of numerical diffusion on isolated bubbles in a gas-solid fluidized bed," *Powder Technology*, **116**, 142-154.

GUENTHER, C., SHAHNAM, M., SYAMLAL, M., LONGANBACH, J., CICERO, D., and SMITH, P., (2002) "CFD Modeling of a Transport Gasifier", Proceedings of the 19th Annual Pittsburgh Coal Conference, Pittsburgh, PA, September 23-27, 2002.

HAYHURST, A.N., and TUCKER, R.F., (1990), "The combustion of carbon monoxide in a two-zone fluidized bed," *Combustion and Flame*, **79**, 175-189.

HESKETH, R.P., and DAVIDSON, J.F. (1991), "Combustion of methane and propane in an incipiently fluidized bed," *Combust. Flame*, **85**, 449-467.

JPL Contract No. 954334 Final Report, (1979) "Feasibility of the silane process for producing semiconductor grade silicon," Union Carbide Corp.

KUNII, D., and LEVENSPIEL, O., (1991) *Fluidization Engineering, 2nd ed.*, Butterworth-Heinemann, Boston.

LEONARD, R., PINKSTON, T., ROGERS, L., RUSH, R., and WHEELDON, J., (2002), "The PSDF—commercial readiness of coal power--revisited" 19th Annual Pittsburgh Coal Conference, Pittsburgh, PA, September 23 - 27, 2002.

McKEEN, T. and PUGSLEY, T.S., (2003) "Simulation of cold flow FCC stripper hydrodynamics at small scale using computational fluid dynamics," *Inter. J. Chemical Reactor Engineering*, **1**: A18.

PRE, P., HEMATI, M., and MARCHAND, B., (1998) "Study on natural gas combustion in fluidized beds: modelling and experimental validation," *Chem. Eng. Sci.*, **53**, 2871-2883.

SNIDER, D.M., O'ROURKE, P.J., and ANDREWS, M.J., (1998), "Sediment flow in inclined vessels calculated using a multiphase particle-in-cell model for dense particle flows," *Inter. J. Multiphase Flow*, **24,** 1359-1382.

SRINIVASAN, R.A., SRIRAMULU, S., KULASEKARAN, S., and AGARWAL, P.K., (1998) "Mathematical modeling of fluidized bed combustion - 2: combustion of gases," *Fuel*, **77**, 1033-1049.

SYAMLAL, M., and BISSET, L., (1992), "METC gasifier advanced simulation (MGAS) model," Technical Note, DOE/METC-92/4108, NTIS/DE92001111, National Technical Information Service, Springfield, VA.

SYAMLAL, M., ROGERS, W., and O'BRIEN, T.J., (1993), "MFIX documentation: theory guide," DOE/METC-94/1004, NTIS/DE94000087, NTIS, Springfield, VA.

SYAMLAL, M., and O'BRIEN, T.J., (2003) "Fluid dynamic simulation of O_3 decomposition in a bubbling fluidized bed" *AIChE J.*, accepted for publication.

van der VAART, D.R., (1992), "Mathematical modeling of methane combustion in a fluidized bed," *Ind. Eng. Chem. Res.*, **31**, 999-1007.